Check for updates

# Experimental study on CO$_2$ capture by MEA/*n*-butanol/H$_2$O phase change absorbent†

Yanlong Hu,[a] Qiang Wang, [ID] *[a] Dingkai Hu,[a] Yingshuang Zhang,[a] Muhammad Furqan[a] and Shijian Lu[b]

Monoethanolamines (MEAs) are widely used for CO$_2$ capture, but their regeneration energy consumption is very high. CO$_2$ Phase change absorbents (CPCAs) can be converted into CO$_2$-rich and CO$_2$-lean phases after absorbing CO$_2$, and the regeneration energy consumption can be reduced because only the CO$_2$-rich phase is thermally desorbed. In this paper, a novel CPCA with the composition "MEA/*n*-butanol/H$_2$O (MNBH)" is proposed. Compared with the reported MEA phase change absorbent, the MNBH absorbent has higher CO$_2$ absorption capacity, smaller absorbent viscosity and CO$_2$-rich phase volume. The MNBH absorbent has the highest CO$_2$ absorption capacity of 2.5227 mol CO$_2$ per mol amine at a mass ratio of 3 : 4 : 3. The CO$_2$ desorption efficiency reaches 89.96% at 120 °C, and the CO$_2$ regeneration energy consumption is 2.6 GJ tCO$_2^{-1}$, which is about 35% lower than that of the 30 wt% MEA absorbent. When the mass ratio of MNBH absorbent was 3 : 6 : 1, the CO$_2$ recycling capacity was 4.1918 mol CO$_2$ L$^{-1}$, which is 76% higher than that of the conventional 30 wt% MEA absorbent. The phase change absorbent developed in this paper can reduce the desorbent volume by about 50% and has good absorption performance for CO$_2$ in flue gas.

## 1. Introduction

CO$_2$ occupies 64% of the total amount of greenhouse gases, and is the main culprit causing the greenhouse effect.[1,2] A large amount of CO$_2$ emissions will gradually increase the surface temperature of the earth, causing many environmental problems such as a catastrophic climate and sea level rise, which will restrict the healthy development of the national economy.[3,4] According to the data released by the International Energy Agency (IEA) in 2022, CO$_2$ emissions from power plants account for 50% of the total emissions.[5] Therefore, CO$_2$ capture in power plants has become very important. Among many CO$_2$ capture technologies in power plants, the chemical absorption method is widely used because of its high CO$_2$ recovery rate, mature process and strong adaptability to coal-fired power plants.[6]

Monoethanolamine (MEA) is widely used in the CO$_2$ capture field, but its regeneration energy consumption is very high.[7] In order to further reduce the energy consumption of CO$_2$ capture by chemical absorption, researchers have developed many new

absorbents, such as mixed amine absorbents, anhydrous absorbents, ionic liquids (ILS) and deep eutectic solvents (DESs). Although these chemical absorbents improved CO$_2$ absorption performance to some extent, there are still some defects such as high energy consumption for CO$_2$ desorption and poor recycling performance of absorbents, which limited their further industrial popularization.

CO$_2$ phase change absorbents (CPCAs) are a new type of CO$_2$ absorbent. Different from organic amine aqueous solution, CPCAs are divided into two phases with different CO$_2$ loading after absorbing CO$_2$. Only the CO$_2$-rich phase loaded with CO$_2$ enters the desorption unit, thus reducing desorption energy consumption. In 2009, the concept of CPCAs was first proposed in the patent published by Liang Hu.[8] Fresh CPCAs are homogeneous phases, but phase separation occurs after absorbing CO$_2$ or changing absorption temperature. One phase where CO$_2$ absorption products are mainly collected is called the CO$_2$-rich phase, and the other phase is called the CO$_2$-lean phase.[9] According to the state of the CO$_2$-rich phase, it can be divided into solid–liquid phase change absorbent and liquid–liquid phase change absorbent. Liquid–liquid phase change absorbent is suitable for conventional chemical absorption process if it is enlarged and put into industry, which has little improvement on traditional absorption devices.[10] Therefore, nowadays, most of the research is mostly focused on the development and application of liquid–liquid phase change absorbents.

Ye[11] explored triethylenetetramine (TETA)/N, N-diethylethanolamine (DEEA) phase change absorbent, and found that its CO$_2$ absorption performance and regeneration energy

*[a]State Key Laboratory of Chemistry and Utilization of Carbon-Based Energy Resources, Xinjiang Key Laboratory of Coal Cleaning Conversion & Chemical Engineering, Xinjiang Uyghur Autonomous Region, School of Chemical Engineering and Technology, Xinjiang University, Urumqi, Xinjiang, 830017, P. R. China. E-mail: wangqiang@xju.edu.cn; Fax: +869918582966*

*[b]Institute of Carbon Neutralization, China University of Mining and Technology, School of Chemical Engineering, Xuzhou, Jiangsu, 221116, China*

† Electronic supplementary information (ESI) available: Supplementary material Associated with this article can be found, in the online version. See DOI: https://doi.org/10.1039/d3ra07193f

consumption were affected by water content. When the water content was 46 wt%, the absorption capacity of the solution was 0.97 mol $CO_2$ per mol amine, and the regeneration energy consumption was 2.98 GJ $t^{-1}$ $CO_2$. Svendsen[12,13] developed phase change absorbents of DEEA and 3-(methylamine) propylamine (MAPA) with energy consumption as low as 2.1 GJ $t^{-1}$ $CO_2$. Huang[14] dissolved amino-functionalized IL-triethylamine tetramine lysine (TETAH] [Lys]) in an ethanol–water solvent. The viscosity of this phase change adsorbent was relatively low, and the $CO_2$ loading in the $CO_2$-rich phase reached 93%. Only one-third of the desorption liquid was sent to the stripper.

MEA is a primary amine, which has many advantages such as low price, fast $CO_2$ absorption rate, relatively high absorption capacity and stable chemical properties, so it is favoured by researchers. At present, MEA-based phase change absorbents have been reported in the literature, including MEA/n-propyl alcohol/$H_2O$, MEA/isopropyl alcohol/$H_2O$ and MEA/tert-butanol/$H_2O$, while the article on MEA/n-butanol/$H_2O$ phase change absorbent has not been reported. In this paper, MEA/n-butanol/$H_2O$ phase change absorbent (denoted as MNBH) was developed with MEA as the main absorbent, n-butanol as the phase separation accelerator, and water as the solvent, and compared with the $CO_2$ absorption performance of existing MEA phase-change absorbents. Then, the $CO_2$ absorption and regeneration properties of MNBH, cyclic regeneration capacity, two-phase material distribution and $CO_2$ capture performance in simulated flue gas were further studied.

## 2. Experimental section

### 2.1 Reagents and instruments

**2.1.1 Experimental reagents.** MEA, analytically pure, was purchased from Aladdin reagents; n-butanol, analytically pure, was purchased from Aladdin Reagents; n-propanol, analytically pure, was purchased from Aladdin reagents; isopropanol, analytically pure, purchased from Tianjin Xinbote Chemical Co; tert-butanol, analytically pure, purchased from Tianjin Xinbute Chemical Co; Hydrochloric acid, 99.7%, Tianjin Zhiyuan Chemical Reagent Co; deionized water, homemade in the laboratory; $CO_2$, 99.99%, purchased from Hepu Beifen Gas Industry Co., Ltd $N_2$, 99.99%, purchased from Beijing Hepu Beifen Gas Industry Co., Ltd $D_2O$ (99.96%), purchased from National Pharmaceutical Chemical Reagent Co., Ltd for nuclear magnetic resonance experiments.

**2.1.2 Experimental equipment.** Digital Viscometer, NDJ-9S, Bangxi Instrument Technology (Shanghai) Co., Ltd; Analytical Balance, GL2202i, Shanghai Li Chen Bang Xi Instrument Technology Co, Ltd; Collector Type Constant Temperature Heating Magnetic Stirrer, DF-101S, Shanghai Li Chen Bang Xi Instrument Technology Co, Ltd; Rotor Flow Meter, LZB-3WB, Changzhou Shuanghuan Thermal Instrument Co, Ltd; Low-temperature coolant circulating pump, DLSB-5/10, Zhengzhou Great Wall Science and Industry Trade Co, Ltd; $CO_2$ loading titration device, self-made in the laboratory; temperature-controlled magnetic stirrer, Jiangsu Jinyi Instrument Science and Technology Co, Ltd; Electrothermal Constant Temperature Blast Drying Oven, DHG-9023A, Shanghai Yiheng Technology Instrument Co., Ltd.

### 2.2 Experimental process

The $CO_2$ absorption experimental device is shown in Fig. 1, and the $CO_2$ desorption experimental device is shown in Fig. 2. Except for the simulated flue gas experiments, all absorption experiments used high-purity $CO_2$ gas. Firstly, the optimal MEA mass concentration is determined. Secondly, the mass concentration of MEA was fixed, the concentration of n-butanol was changed, and the MNBH absorbent with different mass ratio was prepared, and the optimal dosage of n-butanol was determined according to the phase separation behavior and $CO_2$ absorption performance. Under the optimal ratio of MNBH absorbent, the absorption, desorption and recycling ability of MNBH to $CO_2$ were further studied. Finally, FT-IR and $^1H$ NMR techniques were used to analyze the two-phase material distribution of MNBH phase change absorbent, and the phase change mechanism was explained. Finally, the feasibility of MNBH capturing $CO_2$ in flue gas was verified by simulated flue gas experiments.

**2.2.1 $CO_2$ absorption experiment.** The total mass of 20 g of phase change absorption was taken at 30 °C, 1 atm pressure, the flow rate of $CO_2$ is 100 mL $min^{-1}$ and samples were taken every 5 minutes and check the absorption of $CO_2$ in the phase change absorbent by weighing method,[15] and the absorption amount of $CO_2$ is calculated by mathematical formula. When there is no change in the mass of the absorbent or the mass difference between the two weighs is less than 10 mg, we consider that the absorption has reached an equilibrium state. The experiment
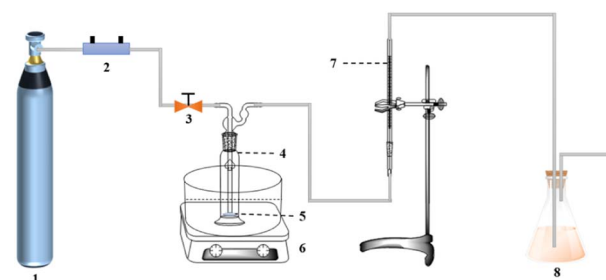


**Fig. 1** Experimental setup for $CO_2$ absorption. (1) $CO_2$ cylinder (2) rotor flow meters (3) valve (4) gas absorption bottle (5) magneton (6) collector-type thermostatic magnetic stirrer (7) soap bubble flow meter (8) tail gas treatment unit.
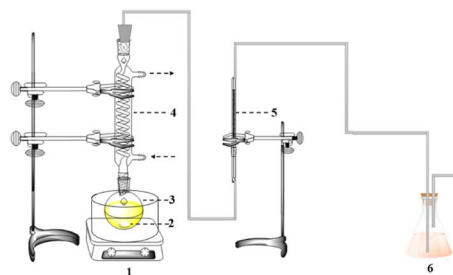


**Fig. 2** $CO_2$ desorption device diagram. (1) Oil bath (2) magneton (3) single mouth flasks (4) snake condenser tube (5) soap bubble flow meter (6) tail gas treatment unit.

was repeated 3 times in each group, and the experimental error was ±3%.

CO$_2$ absorption capacity and absorption rate were used to evaluate the CO$_2$ absorption performance of MNBH. The calculation method of CO$_2$ absorption rate is as shown in formula (1):[16]

$$r_{abs} = \frac{\Delta m}{M_{CO_2} \times \Delta t} \qquad (1)$$

where $r_{abs}$ is the rate of CO$_2$ absorption (mol CO$_2$ min$^{-1}$); $\Delta m$ is the change in mass of the phase change absorption system over time (g); $M_{CO_2}$ is the molar mass of CO$_2$ (g mol$^{-1}$) and $\Delta t$ is the time period corresponding to the change in mass.

The CO$_2$ absorption capacity is calculated as shown in formula (2).[16]

$$R_{total} = \frac{n_{CO_2}}{V_{total}} = \int_0^t r_{abs} dt \qquad (2)$$

In the formula, $R_{total}$ is the CO$_2$ absorption capacity (mol CO$_2$ L$^{-1}$); $n_{CO_2}$ is the molar amount of CO$_2$ (mol); $V_{total}$ is the volume of absorbent (L) and $t$ is the absorption time (min).

The CO$_2$ absorption loading is calculated as shown in formula (3).[17]

$$C_{total} = \frac{(m_2 - m_1)}{M_{CO_2} \times m_{amine}} \qquad (3)$$

where $C_{total}$ is the CO$_2$ absorption loading per mole of amine (mol CO$_2$ per mol amine); $m_1$ is the mass (g) of the absorbing device (absorbing bottle + absorbing tube + absorbent + magneton) before absorption; $m_2$ is the mass (g) of the absorbing device after absorption. $m_{amine}$ is the mass of amine used (g); $M_{amine}$ is the molar mass of amine (g mol$^{-1}$).

**2.2.2 CO$_2$ desorption experiments.** After the absorption experiment, we put the CO$_2$-rich phase into a single-mouth round-bottom flask for the thermal desorption experiment. The desorption experiment will be carried out at 120 °C. A serpentine condensation reflux device is added to minimize losses in the phase change absorption system. To judge whether the desorption process is complete, we use a soap film flow-meter. When the bubbles stop rising and remain for a period, we can assume that desorption has been completely carried out. The repeated experimental error of CO$_2$ desorption is ±3%.

The CO$_2$ desorption performance and cycle capacity of MNBH were investigated by the formula given in formula (4) and (5). CO$_2$ circulation capacity refers to the difference of CO$_2$ capacity before and after desorption of unit volume absorbent (in which CO$_2$ capacity in CO$_2$-lean phase and CO$_2$-rich phase can be measured by titration) formula (4) Shown in:[18]

$$\Delta R = R_{bde} - R_{ade} \qquad (4)$$

where $\Delta R$ is the CO$_2$ cycle capacity (mol CO$_2$ L$^{-1}$); $R_{bde}$ is the CO$_2$ capacity in the CO$_2$-rich phase before desorption (mol CO$_2$ L$^{-1}$); $R_{ade}$ is the CO$_2$ capacity in the CO$_2$-rich phase after desorption (mol CO$_2$ L$^{-1}$).

The desorption efficiency is calculated as shown in formula (5):[18]

$$\eta = \frac{\Delta R}{R_{bde}} = \frac{R_{bde} - R_{ade}}{R_{bde}} \qquad (5)$$

where $\eta$ is the CO$_2$ desorption efficiency.

**2.2.3 Simulated flue gas experiment.** The experimental setup of MNBH for capturing CO$_2$ in flue gas is shown in Fig. 3 the simulated flue gas consists of 15 vol% CO$_2$ and 85 vol% N$_2$. The simulated flue gas is passed into a gas mixer and mixed evenly. The rotor flowmeter is used to control the flue gas flow rate to 100 mL min$^{-1}$. The experimental method is the same as 2.2.1. The reproducibility error of simulated flu gas test is ±5%.

**2.2.4 CO$_2$ loading measurement experiment.** Fig. 4 shows a specific instrument setup for measuring CO$_2$ loading in lean and CO$_2$-rich phase in the laboratory. Based on the principle of placing strong acid in weak acid, 0.2 mL upper and lower liquid phase was taken into a conical bottle after CO$_2$ absorption ended, and the initial reading $V_2$ of the U-shaped tube was recorded. Use an excess of 2 mol L$^{-1}$ dilute hydrochloric acid for titration until the hydrochloric acid level in the U-shaped tube no longer changes, record the reading $V_3$ at that time, and calculate the usage amount $V_1$ of dilute hydrochloric acid at the same time.

The calculation method of CO$_2$ loading in CO$_2$-rich and CO$_2$-lean phase is shown in formula (6).[19] The repetition error of CO$_2$ loading test was ±5%.

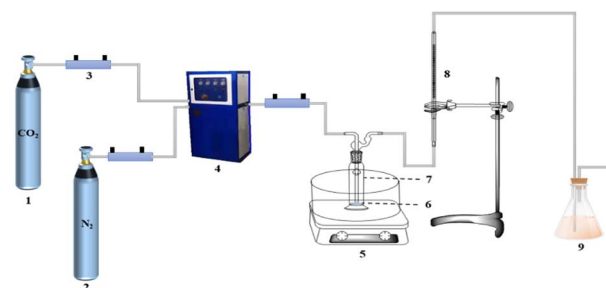$$L = \frac{V_3 - V_2 - V_1}{24.5 \times V_0} \qquad (6)$$



**Fig. 3** Simulated flue gas experimental setup. (1) CO$_2$ cylinder (2) N$_2$ cylinder (3) rotor flow meter (4) gas mixer (5) collector type constant temperature magnetic stirrer (6) magneton (7) gas absorption cylinder (8) soap bubble flow meter (9) tail gas treatment device.
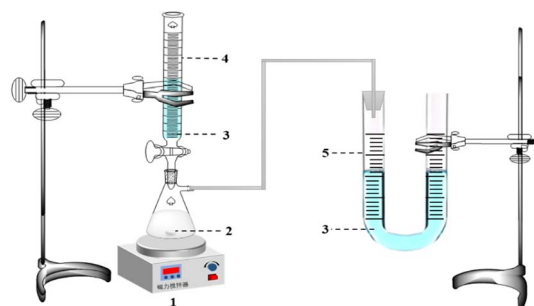


**Fig. 4** Depleted-CO$_2$-rich phase CO$_2$ loading measurement device. (1) magnetic stirrer (2) magnets (3) dilute hydrochloric acid (4) acid burette (5) U-tube.

$L$ is the $CO_2$ loading in the lean or $CO_2$-rich phase (mol $CO_2$ $L^{-1}$); 24.5 refers to the volume corresponding to 1 mol of gas at room temperature; $V_0$ refers to the volume of solution to be measured (mL); $V_1$ refers to the amount of 2 mol $L^{-1}$ dilute hydrochloric acid (mL); $V_2$ refers to the initial U-tube reading (mL); $V_3$ refers to the U-tube reading at the end of the titration (mL).

**2.2.5 Infrared spectroscopy experiments.** In this paper, the change of infrared spectral characteristic peaks before and after $CO_2$ absorption and desorption was investigated by an infrared spectrometer (model VERTEX). The spectral test range used is 4000–400 $cm^{-1}$.

**2.2.6 Nuclear magnetic resonance experiments.** We used $^1H$ NMR (model JEOL JNM-AL400), to analyse the material distribution before and after $CO_2$ absorption. Deuterated water ($D_2O$) was used as a solvent.

**2.2.7 Estimation of renewable energy consumption.** The regeneration energy ($Q_{reg}$, GJ $tCO_2^{-1}$) consists of three parts: reaction heat ($\Delta H_{abs}$), sensible heat ($Q_{sens}$) for solutions heating up and latent heat ($Q_{latent}$) for water evaporation, as shown in formula (7).[20]

$$Q_{reg} = \Delta H_{abs} + Q_{sens} + Q_{latent} \quad (7)$$

The $\Delta H_{abs}$ is measured in two ways, either by a calorimeter or by the Gibbs Helmholtz equation. In this paper, the gas–liquid equilibrium experimental device used by Xiao[21] et al. and Zhang[22] et al. was used to measure the $CO_2$ equilibrium solubility of each amine solvent at different temperatures and different $CO_2$ partial pressures, and the $\Delta H_{abs}$ was calculated by Gibbs Helmholtz equation. The Gibbs Helmholtz equation is shown in formula (8):

$$\frac{d(\ln P_{CO_2})}{d\left(\frac{1}{T}\right)} = \frac{\Delta H_{abs}}{R} \quad (8)$$

where $P_{CO_2}$ is the partial pressure of $CO_2$, kPa; $T$ is the reaction temperature, K; $\Delta H_{abs}$ is the heat of reaction, kJ $mol^{-1}$; $R$ is the gas constant, 8.314 J ($mol^{-1}$ $K^{-1}$).

$Q_{sens}$ is the energy required to heat the $CO_2$-rich phase from the absorption temperature to the desorption temperature. It can be calculated using formula (9):[17]

$$Q_{sens} = \frac{m_L(C_{am} + r_w C_w + \alpha_{lean} C_{CO_2})\Delta T}{m_{CO_2}} \quad (9)$$

where $m_L$ is the total mass of the solution in the regeneration process; g; $C_{am}$, $C_w$ and $C_{CO_2}$ (kJ ($mol^{-1}$ $K^{-1}$)) are the heat capacities of MEA, $H_2O$ and $CO_2$, respectively; $r_w$ is the molar ratio of water to MEA in fresh absorbent; $\alpha_{lean}$ (mol $CO_2$ per mol amine) is the $CO_2$-lean phase loading after absorption; $\Delta T$ (K) is the temperature difference between the top and bottom of the desorption tower, generally 10 K.

$Q_{latent}$ refers to the amount of energy to be absorbed by partial solvents such as water and n-propanol for generating steam at 393.15 K of rich phase. Which can be calculated by formula (10):[17]
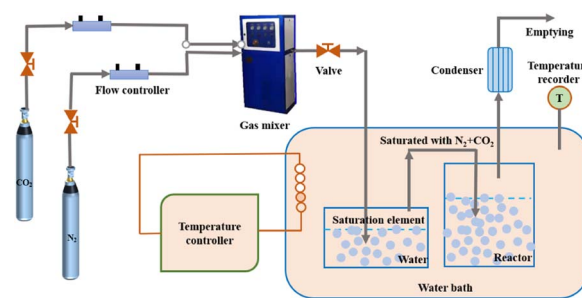
$$Q_{latent} = m_w \lambda \quad (10)$$



**Fig. 5** Schematic diagram for the measurement of $CO_2$ equilibrium solubility.

where $m_w$ (mol) is the number of moles of water vapour in the stream at the outlet of the stripper, $\lambda$ (kJ $mol^{-1}$) is the latent heat of the water.

$m_w$ is calculated by formula (11):

$$m_w = \frac{MP_w(T_{top})}{P^*_{CO_2}(T_{top})} \quad (11)$$

where $M$ (kmol $tCO_2^{-1}$) is the number of moles per ton of $CO_2$; $P_w(T_{top})$ is the partial pressure of water vapour at the top temperature of a stripper; $P^*_{CO_2}(T_{top})$ is the $CO_2$ partial pressure at the top temperature of the stripper.

**2.2.8 $CO_2$ equilibrium solubility measurements.** The gas–liquid balancing device is shown in Fig. 5. The $CO_2$ equilibrium solubility measuring device consists of a gas supply system, a reaction system and a condenser. The flue gas simulation gas consisted of $N_2$ and $CO_2$, and the flue gas flow rate was 300 mL $min^{-1}$. The corresponding flow rate and the required $CO_2$ partial pressure were regulated by a flow controller.

## 3. Results and discussion

N-Butanol is an excellent alcohol organic solvent, which has the characteristics of low price and low viscosity. This makes it a very popular phase separator. Compared with n-propanol, isopropanol and tert-butanol, n-butanol has low saturated vapour pressure. The saturated vapour pressure values of n-propanol, isopropanol, tert-butanol and n-butanol at 1 atm, 0–
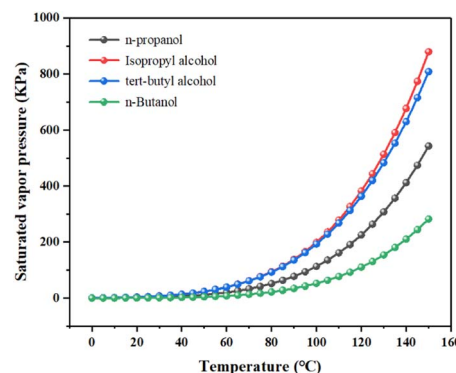


**Fig. 6** Comparison diagram of saturated vapor pressure of several alcohols.

**Table 1** Result of Absorption Experiment

| Phase separation solvent | Whether phase is separated | Absorption capacity (mol $CO_2$ $L^{-1}$) | Equilibrium time (min) | Viscosity (mPa s) | Percentage of $CO_2$-rich phase volume (%) | Ref. |
|---|---|---|---|---|---|---|
| *n*-Propanol | Yes | 2.1567 | 25 | 12.10 | 59 | 19 |
| Isopropanol | Yes | 1.9911 | 20 | 10.12 | 64 | 19 |
| *Tert*-butyl alcohol | Yes | 1.8902 | 20 | 11.68 | 55 | 23 |
| *n*-Butanol | Yes | 2.4081 | 35 | 8.86 | 50 | This work |

150 °C (temperature range increment is 5 °C) were obtained by Aspenplus simulation. In the study of physical properties, the physical properties method was chosen as NRTL (Non-Random Two-Liquid). Fig. 6 shows our simulation results.

It can be seen from Fig. 6 that *n*-butanol has the lowest saturated vapour pressure compared with other alcohols, Therefore, using *n*-butanol as a phase separation accelerator is more conducive to reducing the volatilization loss of phase change system.

The total mass of the phase change system was selected as 20 g, and the mass ratio of each component in the phase change system was 3 : 4 : 3. Under the experimental conditions of absorption temperature of 30 °C, 1 atm, and $CO_2$ flow rate of 100 mL min$^{-1}$, the experimental results of the absorption of pure $CO_2$ by the four phase change absorbents are shown in Table 1.

It can be seen from Table 1 that all the four absorption systems can be divided into phases after absorbing $CO_2$ to saturation, with MNBH absorbent having the highest $CO_2$ absorption capacity and the lowest viscosity of the absorbent. In addition, the $CO_2$-rich phase volume of MNBH absorbent only accounts for 50% of the total absorbent volume, which will greatly reduce the energy consumption of the desorption unit.[24] The distribution of rich and $CO_2$-lean phase volume in the four-phase change systems is shown in Fig. 7.

The comparison of $CO_2$ absorption capacity and absorption rate of the four-phase change system is shown in Fig. 8.

From Fig. 8a, the phase change system with *n*-butanol as the phase separation promoter has the highest $CO_2$ absorption capacity, and the order of $CO_2$ absorption capacity is MEA/*n*-butanol/$H_2O$ > MEA/*n*-propanol/$H_2O$ > MEA/isopropanol/$H_2O$ >

MEA/*tert*-butanol/$H_2O$. From Fig. 8b that the order of $CO_2$ absorption rate is MEA/*tert*-butanol/$H_2O$ > MEA/*n*-propanol/$H_2O$ > MEA/*n*-butanol/$H_2O$ > MEA/isopropanol/$H_2O$ during the first 5 min of absorption, and the order of $CO_2$ absorption rate after 15 min is as follows: MEA/*n*-butanol/$H_2O$ > MEA/*n*-propanol/$H_2O$ > MEA/isopropanol/$H_2O$ > MEA/*tert*-butanol/$H_2O$. The phase separation phenomenon of the four-phase change systems after absorbing $CO_2$ saturation is shown in Fig. 9.

In summary, compared with several other MEA phase change absorption systems, the MNBH absorbent has the highest $CO_2$ absorption capacity, the lowest viscosity of the absorbent, and the volume of the $CO_2$-rich phase at absorption equilibrium is only 50% of the total volume. Therefore, it is more advantageous to choose *n*-butanol as the phase separation promoter to develop MNBH in this paper.

### 3.1 Optimization of mass concentration of MEA

Before exploring the optimum mass ratio of the MNBH absorption system, the optimum mass concentration of MEA needs to be determined. Based on the literature reports and the actual industrial applications of MEA, the mass concentrations of MEA were selected as 20 wt%, 30 wt%, 40 wt%, and 50 wt%,
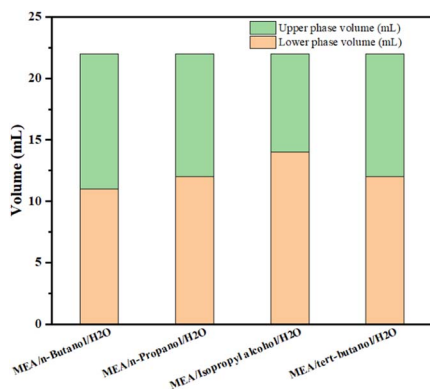
**Fig. 8** (a) The variation of $CO_2$ absorption capacity with time; (b) $CO_2$ absorption rate varies with time.

**Fig. 7** Depleted and enriched liquid volume distribution.
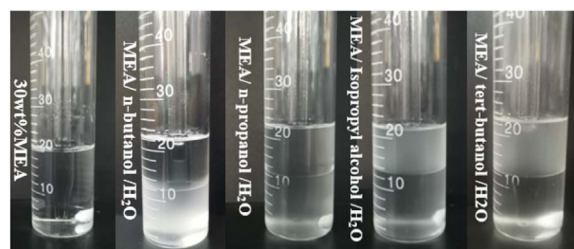
**Fig. 9** Split-phase diagram of four phase change systems after absorbing $CO_2$ to saturation.

**Table 2** $CO_2$ absorption results of different mass concentration of MEA

| MEA mass concentration | Absorption loading (mol $CO_2$ per mol amine) | Absorption capacity (mol $CO_2$ L$^{-1}$) | Equalization time (min) | Absorbent viscosity (mPa s) |
|---|---|---|---|---|
| 20 wt% | 0.6132 | 2.0106 | 50 | 2.12 |
| 30 wt% | 0.5779 | 2.8382 | 60 | 3.44 |
| 40 wt% | 0.5438 | 3.5610 | 70 | 6.22 |
| 50 wt% | 0.5243 | 4.2918 | 90 | 13.65 |
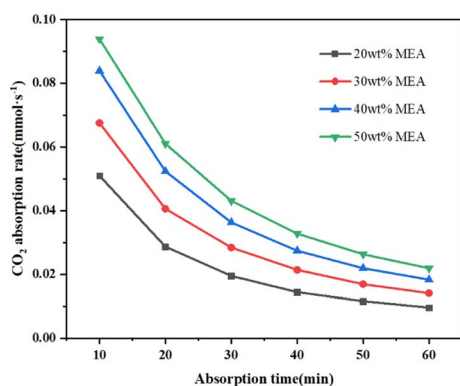


**Fig. 10** Comparison of $CO_2$ absorption rates for different mass concentrations of MEA.

in that order. Under the experimental conditions of 30 °C, 1 atm, and $CO_2$ rate of 100 mL min$^{-1}$, the results of $CO_2$ absorption experiments are shown in Table 2.

The utilization of amine can be expressed in terms of mol $CO_2$ per mol amine.[17] As can be seen from Table 2, with the increase of MEA mass concentration, $CO_2$ absorption capacity and absorbent viscosity increase, the time required for absorption to reach equilibrium becomes longer, and the utilization rate of MEA decreases. As 30 wt% MEA has a higher $CO_2$ absorption capacity and MEA utilization, the viscosity of the absorbent is lower at 3.44 mpa s, and the time to equilibrium is shorter at 60 min. Therefore, 30 wt% MEA was chosen as a suitable mass concentration, which is also consistent with the recommended MEA mass concentration in the literature.[19]

Fig. 10 shows the $CO_2$ absorption rate curves corresponding to different MEA mass concentrations. From the Fig. 10, the $CO_2$ absorption rate increases with the increase of MEA concentration.

### 3.2 Optimization of mass ratio of MEA/$n$-butanol/H$_2$O system

The mass concentration of MEA was fixed at 30 wt%, $m_{(MEA)}$ : $m_{(n\text{-butanol})}$ : $m_{(H_2O)}$ were mixed in the mass ratios of 3 : 1 : 6, 3 : 2 : 5, 3 : 3 : 4, 3 : 4 : 3, 3 : 5 : 2, 3 : 6 : 1, and 3 : 7 : 0 to form an eight-group absorption system. The total mass of the phase change absorption system was taken as 20 g, at 25 °C, 1 atm, and the $CO_2$ inlet flow rate of 100 mL min$^{-1}$, the $CO_2$ absorption results of the MNBH systems with different mass ratios are shown in Table 3.

It can be seen from Table 3 that phase transition can occur if $n$-butanol is added, which can also be said that $n$-butanol plays the role of phase separation accelerator in the phase transition system. The viscosity of the phase transition system increases with the increase of the mass concentration of $n$-butanol, and the viscosity of the upper liquid phase is maintained at about 2.60 mPa s, while the data show that the viscosity of $n$-butanol at room temperature is 2.55 mPa s. Therefore, it is speculated that the main composition of the upper liquid phase is $n$-butanol, which is a $CO_2$-lean phase.

Fig. 11 shows the comparison of $CO_2$ absorption capacity and $CO_2$ absorption rate of MNBH with different mass ratios.

From Fig. 11, the $CO_2$ absorption capacity of MNBH increased and then decreased with the increase of $n$-butanol dosage. When the mass ratio of MNBH was 3 : 4 : 3, the maximum $CO_2$ absorption capacity was 2.5227 mol $CO_2$ L$^{-1}$. The $CO_2$ absorption rates were close at different mass ratios. The density and $CO_2$ loading data of the upper and lower phases were measured and the results are shown in Table 4.

As shown in Table.4. The density of the upper phase of MNBH is stable at about 0.75 g mL$^{-1}$, while the density of the lower phase increases with the increase of the mass concentration of $n$-butanol. The density of $n$-butanol is about 0.81 g mL$^{-1}$ at room temperature, and the density of the upper phase

**Table 3** $CO_2$ absorption results of MEA/$n$-butanol/H$_2$O system with different mass ratios

| Mass ratios | Whether phase is separated | Percentage of $CO_2$-rich phase volume (%) | $CO_2$ absorption capacity (mol $CO_2$ L$^{-1}$) | Absorbent viscosity (mPa s) | Upper phase viscosity (mPa s) | Lower phase viscosity mPa s) |
|---|---|---|---|---|---|---|
| 3 : 1 : 6 | Yes | 90 | 2.4184 | 4.29 | 2.63 | 7.29 |
| 3 : 2 : 5 | Yes | 71 | 2.4370 | 4.80 | 2.59 | 8.79 |
| 3 : 3 : 4 | Yes | 62 | 2.4476 | 6.26 | 2.61 | 10.17 |
| 3 : 4 : 3 | Yes | 50 | 2.5227 | 8.18 | 2.67 | 13.46 |
| 3 : 5 : 2 | Yes | 46 | 2.4909 | 11.60 | 2.65 | 16.98 |
| 3 : 6 : 1 | Yes | 38 | 2.4424 | 13.52 | 2.64 | 19.12 |
| 3 : 7 : 0 | Yes | 19 | 2.3843 | — | 2.60 | 38.12 |
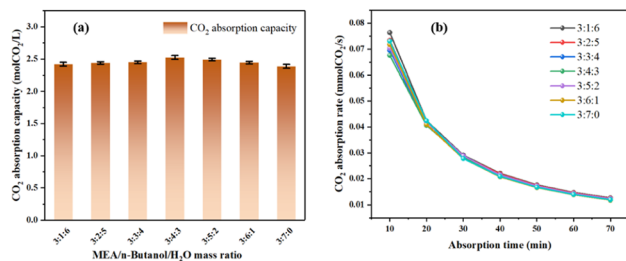
**Fig. 11** (a) Comparison of $CO_2$ absorption capacity; (b) comparison of $CO_2$ absorption rate.



**Fig. 12** Distribution of $CO_2$-rich and $CO_2$-lean phase volume.

of MNBH is very close to the density value of *n*-butanol at room temperature. In addition, the $CO_2$ loading of the lower phase of the MNBH absorbent reaches more than 95% at all mass ratios. Therefore, we can speculate that after the absorption of $CO_2$ by MNBH, the $CO_2$ absorption products are mainly concentrated in the lower phase, which is a $CO_2$-rich phase, while the upper phase is mainly composed of *n*-butanol, which is a $CO_2$-lean phase.

Theoretically, only the $CO_2$-rich phase needs to be sent to the desorption unit when the phase change absorbent is thermally regenerated. Therefore, the small $CO_2$-rich phase volume is helpful to reduce the regeneration energy consumption. The upper and lower phase volume distribution of MNBH with different mass ratios after absorbing $CO_2$ to saturation is shown in Fig. 12. It can be known that with the increase of *n*-butanol dosage, the volume of the lower phase gradually decreases.

In summary, when the mass ratio of MNBH is 3 : 4 : 3, the $CO_2$ absorption capacity is the highest, the viscosity of the absorbent is 8.18 mpa s, and the viscosity of the rich phase is 13.46 mpa s. The volume of the $CO_2$-rich phase was only 50% of the total volume of the absorbent, which greatly reduced the energy consumption for absorbent regeneration. Therefore, 3 : 4 : 3 was selected as the optimum mass ratio. The phenomena before and after phase separation of MNBH with 3 : 4 : 3 mass ratio is shown in Fig. 13.

### 3.3 CO2 absorption properties of MNBH

**3.3.1 Effect of absorption temperature on absorption performance.** Under the experimental conditions of 1 atm and $CO_2$ rate of 100 mL min$^{-1}$, the mass ratio of fixed MNBH is 3 : 4 : 3, and the $CO_2$ absorption experiments are carried out at the
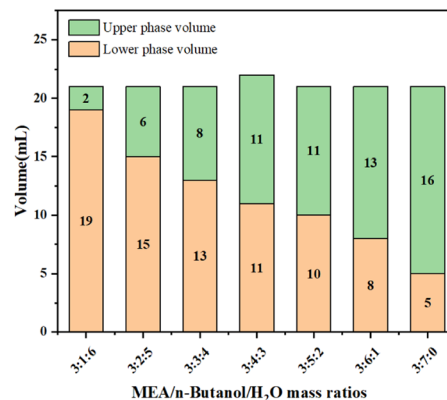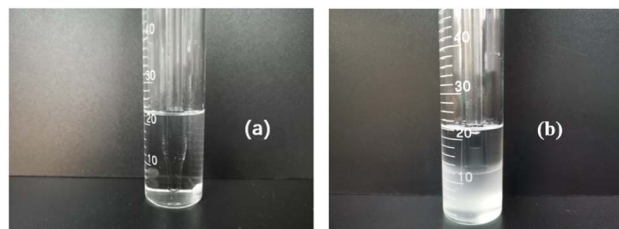


**Fig. 13** (a) Before $CO_2$ absorption by MNBH; (b) after $CO_2$ absorption by MNBH.

temperature of 20 °C, 30 °C, 40 °C and 50 °C in sequence. The experimental results are shown in Fig. 14.

From Fig. 14a, the $CO_2$ absorption capacity of the MNBH absorbent with a mass ratio of 3 : 4 : 3 decreases slightly with the increase in temperature. From Fig. 14b, the temperature does not have much effect on the $CO_2$ absorption capacity. When the actual flue gas captures $CO_2$, the temperature at which the flue gas reaches the absorption tower is about 30–50 °C,[25] which indicates that the phase change absorbent developed in this paper has good industrial practical application value. In addition, the higher the absorption temperature, the shorter the time required for absorption to reach equilibrium. After comprehensive consideration, 40 °C is chosen as the best absorption temperature.

**3.3.2 Effect of CO2 partial pressure on absorption performance.** In actual industrial production, the $CO_2$ content in flue

**Table 4** Upper and lower phase density and $CO_2$ loading data for different mass ratios of MNBH

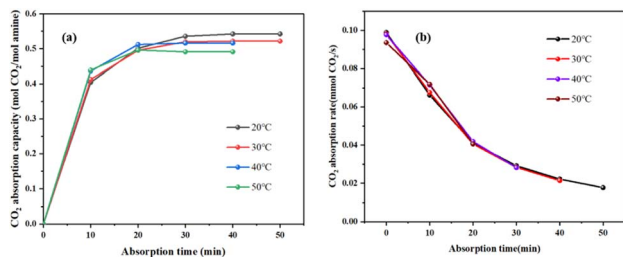| Mass ratios | Upper phase density (g mL$^{-1}$) | lower phase density (g mL$^{-1}$) | Upper phase $CO_2$ loading (mol $CO_2$ L$^{-1}$) | Lower phase $CO_2$ loading (mol $CO_2$ L$^{-1}$) |
|---|---|---|---|---|
| 3 : 1 : 6 | 0.7924 | 1.0011 | 0.1361 | 3.0612 |
| 3 : 2 : 5 | 0.7345 | 1.0017 | 0.0865 | 3.0416 |
| 3 : 3 : 4 | 0.7408 | 1.0263 | 0.1296 | 3.0298 |
| 3 : 4 : 3 | 0.7307 | 1.0620 | 0.1162 | 3.0175 |
| 3 : 5 : 2 | 0.7493 | 1.0991 | 0.0936 | 3.0006 |
| 3 : 6 : 1 | 0.7536 | 1.1508 | 0.1276 | 2.9989 |
| 3 : 7 : 0 | 0.7426 | 1.2012 | 0.1348 | 2.9879 |

**Fig. 14** (a) Curve of $CO_2$ absorption capacity changing with time; (b) curve of $CO_2$ absorption rate changing with time.
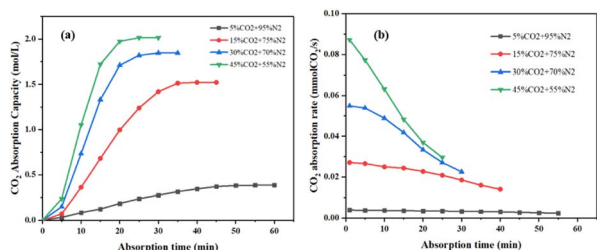


**Fig. 15** (a) Effect of $CO_2$ partial pressure on absorption capacity; (b) effect of $CO_2$ partial pressure on absorption rate.

gas is about 15 vol% $CO_2$ + 85 vol% $N_2$.[26] Therefore, the partial pressure of $CO_2$ in the flue gas was changed to study the effect of $CO_2$ partial pressure on the absorption performance of MNBH. The experimental results are shown in Fig. 15.

From Fig. 15, with the increase of $CO_2$ partial pressure, the $CO_2$ absorption capacity and absorption rate increase, and the absorption time to reach equilibrium is shortened. When the partial pressure of $CO_2$ in the flue gas is 15 vol% $CO_2$, the MNBH absorbent still has good $CO_2$ absorption performance, the $CO_2$ absorption capacity is 1.5961 mol $CO_2$ $L^{-1}$, and the initial $CO_2$ absorption rate is 0.0271 mmol $CO_2$ $s^{-1}$. This shows that the MNBH still has a good absorption capacity in the low partial pressure $CO_2$ environment.

## 3.4 Desorption performance of $CO_2$ by MNBH

### 3.4.1 Effect of desorption temperature on desorption performance.
In the desorption process, a high desorption temperature means an increase in energy consumption in the desorption process.[27] Separate the $CO_2$-lean phase and the $CO_2$-rich phase and seal the $CO_2$-lean phase for later use. A $CO_2$-rich phase will be fed into the desorption device for thermal desorption. The $CO_2$-rich phase is desorbed under 90 °C, 100 °C, 110 °C, 120 °C, 130 °C, 140 °C in oil bath. The calculation method of desorption efficiency is shown in formula (5). The Fig. 16 shows the variation trend of $CO_2$ desorption efficiency with temperature.

It can be seen from Fig. 16 that the desorption efficiency of $CO_2$ increases with the increase of desorption temperature. When the desorption temperature is 120 °C, the desorption efficiency reaches 89.96%. When the desorption temperature rises to 130 °C, the desorption efficiency is 91.32%. The
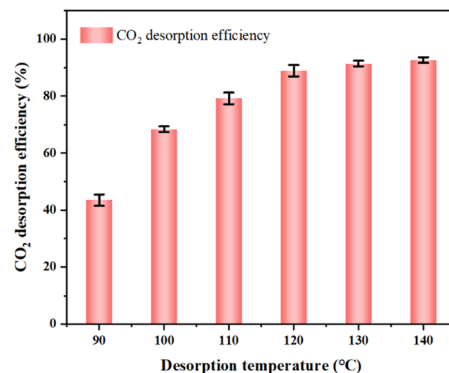


**Fig. 16** Variation of $CO_2$ desorption efficiency with temperature.

desorption efficiency did not increase significantly. Therefore, considering the energy consumption of thermal desorption, selecting the regeneration temperature to 120 °C.

### 3.4.2 Desorption energy consumption.
As shown in Fig. 17, the equilibrium solubility of the 30 wt% MEA absorbent and the MNBH absorbent with a mass ratio of 3 : 4 : 3 was tested using a $CO_2$ equilibrium solubility measurement device at different $CO_2$ partial pressures and temperatures.

As shown in Fig. 18, temperatures ($T$) and pressures ($P_{CO_2}$) corresponding to the same $CO_2$ loading were selected from the data in Fig. 17, and then plotted linearly between $\ln(P_{CO_2})$ and $1/T$. Multiply the slope of the line shown in the diagram by the gas constant 8.314 J $(mol^{-1}$ $K^{-1})$ to get the corresponding $\Delta H_{abs}$.[21]

As calculated from Fig. 18a, 30 wt% MEA absorbent $\Delta H_{abs}$ is 82.1 kJ $mol^{-1}$. This is like the 83 kJ $mol^{-1}$ data reported by Kim et al.,[28] indicating that it is feasible to determine heat
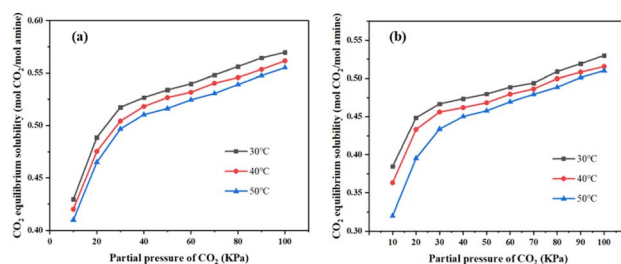


**Fig. 17** (a) 30 wt% MEA absorbent $CO_2$ equilibrium solubility; (b) $CO_2$ equilibrium solubility of MNBH absorbent with mass ratio of 3 : 4 : 3.
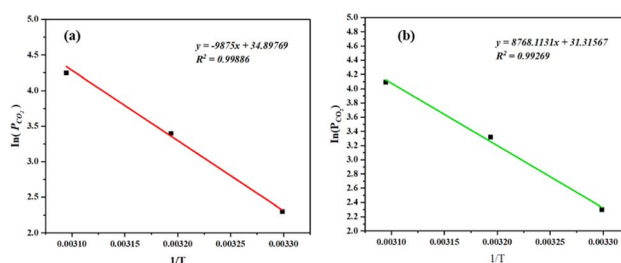


**Fig. 18** (a) 30 wt% MEA absorbent $\Delta H_{abs}$ calculation; (b) calculation of MNBH absorbent $\Delta H_{abs}$ with mass ratio of 3 : 4 : 3.

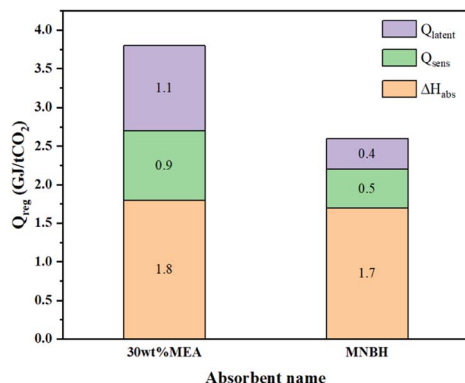Fig. 19  Comparison of renewable energy consumption.

absorption by $CO_2$ using the device shown in Fig. 5. The $\Delta H_{abs}$ of the MNBH phase change absorbent with a mass ratio of 3 : 4 : 3 was calculated from Fig. 18b to be 49.09 kJ mol$^{-1}$.

Combining the calculation formulas of $\Delta H_{abs}$, $Q_{sens}$ and $Q_{latent}$, the desorption energy consumption of MNBH phase change absorbent with mass ratio of 3 : 4 : 3 is estimated and compared with 30 wt% MEA absorbent. The results are shown in Fig. 19.

Fig. 19 shows that the $Q_{sens}$ of MNBH absorbent is 44% lower than that of 30 wt% MEA absorbent, and the $Q_{latent}$ of MNBH absorbent is 64% lower than that of 30 wt% MEA absorbent. The total regenerative energy consumption of MNBH absorbent is 2.6 GJ t$^{-1}$ $CO_2$, which is 35% lower than that of 30 wt% MEA absorbent (3.8 GJ t$^{-1}$ $CO_2$).[28]

## 3.5  Recycling ability of MNBH

In the industrial $CO_2$ capture process, the absorbent needs to be recycled between the absorption and desorption towers.[24] Therefore, the absorbent with high $CO_2$ recycling capacity is more conducive to the $CO_2$ capture process, so the recycling capacity is often taken as an important index when evaluating the absorbent performance. The $CO_2$ cycling capacity of MNBH with mass ratios of 3 : 1 : 6–3 : 7 : 0 were determined at an absorption temperature of 40 °C and a desorption temperature of 120 °C, as shown in Fig. 20a. In addition, MNBH with a mass ratio of 3 : 4 : 3 was regenerated by four absorption–desorption cycles under the above conditions, and its $CO_2$ cycling capacity was measured and compared with the 30 wt% MEA absorbent, as shown in Fig. 20b.
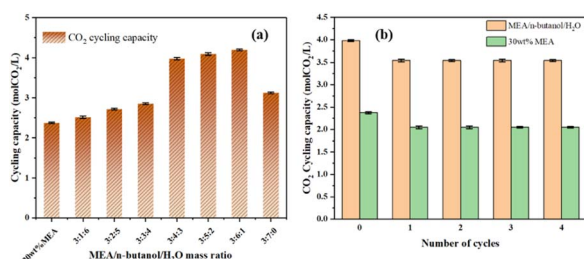
It can be seen from Fig. 20a that with the increase of *n*-butanol concentration, the $CO_2$ recycling capacity of MNBH first increased and then decreased. Compared with 30 wt% MEA absorbent, when MNBH mass ratio is 3 : 4 : 3, the $CO_2$ cycle capacity is improved by 67%. The highest $CO_2$ cycling capacity was achieved at a mass ratio of 3 : 6 : 1, which resulted in a 72% increase in $CO_2$ cycling capacity compared to the 30 wt% MEA absorbent.

As shown in Fig. 20b, in all four absorption-desorption cycling experiments, the $CO_2$ cycling capacity of the MNBH absorber with a mass ratio of 3 : 4 : 3 was higher than that of the 30 wt% MEA absorbent. The $CO_2$ cycle capacity of MNBH decreases somewhat after the first cycle and is stable at about 3.5 mol $CO_2$ L$^{-1}$ in the subsequent cycle. In four cycles, the total circulating capacity of MNBH is 14.1672 mol $CO_2$ L$^{-1}$, which is 5.9752 mol $CO_2$ L$^{-1}$ higher than that of 30 wt% MEA absorbent. This indicates that MNBH has a higher $CO_2$ cycle capacity, that is, it has good cycle stability, and is a promising $CO_2$ absorbent.

## 3.6  Explanation of phase transition mechanism

### 3.6.1  Infrared spectral characterization.
Fig. 21 shows the FT-IR results of the $CO_2$-rich phase before $CO_2$ absorption, after $CO_2$ absorption and after desorption of MNBH with a mass ratio of 3 : 4 : 3.

As can be seen from Fig. 21, in the infrared spectrum of fresh MNBH, the O–H stretching vibration peak appears at 3353 cm$^{-1}$, the C–H stretching vibration peak appears at 2940 cm$^{-1}$, and the methyl stretching vibration peak appears at 2880 cm$^{-1}$.[29] The characteristic peaks at 2151 cm$^{-1}$ and 1579 cm$^{-1}$ can be attributed to the bending vibration of the N–H bond on the amino group (–NH$_2$) in the amine molecule. A weaker acromion is also observed at about 1648 cm$^{-1}$, representing a characteristic peak of the amine cation (–NH$_3^+$).[30,31] When $CO_2$ is absorbed by the phase change absorbent, the acromion at 1648 cm$^{-1}$ is enhanced, which may be due to the overlap between the carbonyl (C=O) stretching vibration peak and the –NH$_3^+$ peak.[32] This result shows that carbamate products are formed in the absorption system after the reaction of phase change absorbent with $CO_2$. After desorption, the peaks of 3353 cm$^{-1}$, 2940 cm$^{-1}$ and 2880 cm$^{-1}$ re-emerged. This means that the carbamate is decomposed into MEA.



Fig. 20  (a) Comparison chart of recycling capacity; (b) comparison of four sorbation–desorption cycle regeneration experiments.
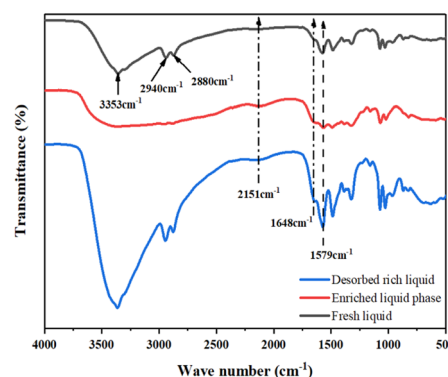


Fig. 21  Infrared spectra of phase change absorbents.

**Table 5** The hydrogen atoms are numbered

| Component | Structure and identification |
| --- | --- |
| MEA/MEAH$^+$ | |
| MEACOO$^-$ | |
| n-Butanol | |

**3.6.2  $^1$H NMR characterization.** The main substances and absorption products of the phase change system were numbered by hydrogen atoms, as shown in Table 5.

Fig. 22 shows the $^1$H NMR results of the upper liquid phase and lower liquid phase of MNBH with a mass ratio of 3 : 4 : 3 before absorbing $CO_2$ and after absorbing $CO_2$ to saturation.

As can be seen from Fig. 22a, there are both characteristic peaks of MEA (1 and 2) and n-butanol (5, 6, 7 and 8) in the fresh
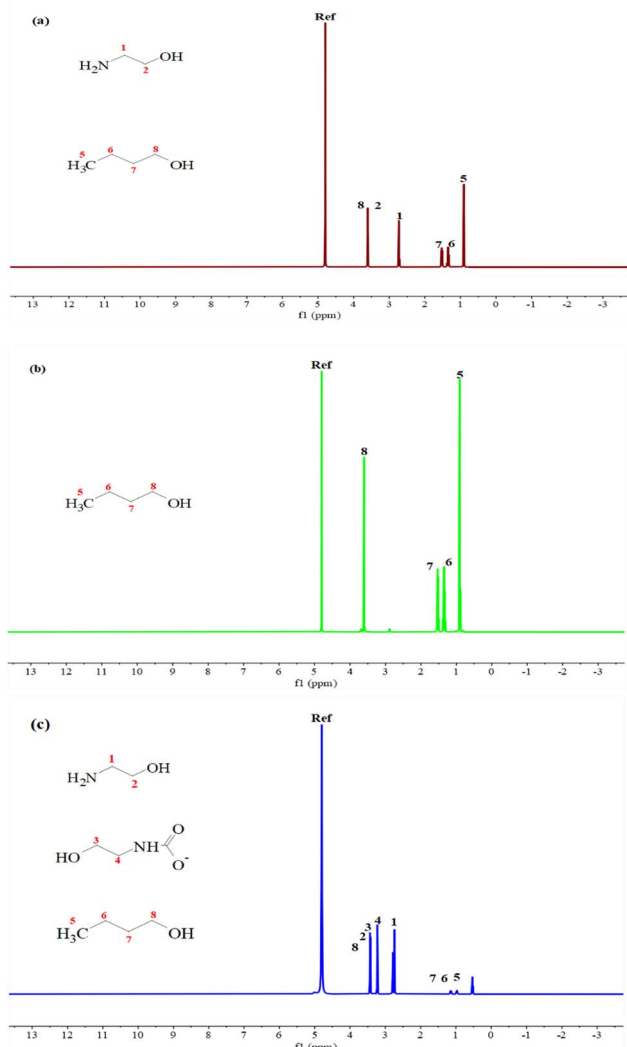


**Fig. 22**  $^1$H NMR of MNBH with a mass ratio of 3 : 4 : 3 (a) before $CO_2$ absorption; (b) upper liquid phase; (c) lower liquid phase.
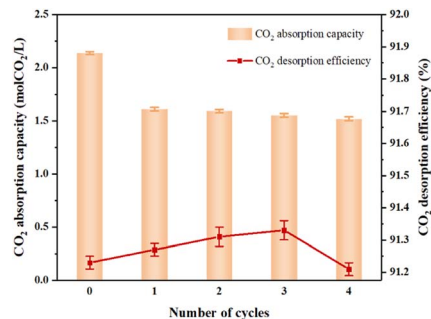


**Fig. 23** Cyclic regeneration experiment under simulated flue gas environment.

solution before $CO_2$ absorption. Due to the rapid exchange of protons with water, the signals of MEA and protonated MEA cannot be distinguished.[33–35] According to Fig. 22b, the upper liquid phase presents only the characteristic peak of n-butanol with relatively high peak intensity, which indicates that the main component of the upper liquid phase is n-butanol. Fig. 22c shows that in the lower liquid phase after $CO_2$ absorption to saturation, there are two more characteristic peaks (3 and 4) at the chemical shifts of 3.06 ppm and 3.55 ppm, which can be attributed to carbamate.[36] In addition, there are MEA characteristic peaks and weak peak intensity n-butanol characteristic peaks in the lower liquid phase This shows that the lower liquid phase is a $CO_2$-rich phase, mainly composed of MEA and carbamate, and contains a small amount of n-butanol, which may be caused by incomplete liquid separation during liquid separation operation.

## 3.7  Simulated flue gas experiments

The total flue gas flow was controlled as 100 mL min$^{-1}$, and the simulated flue gas composition was 15 vol% $CO_2$ + 85 vol $N_2$. Four regeneration experiments were carried out under the conditions of absorption temperature of 40 °C and desorption temperature of 120 °C, and the experimental results are shown in Fig. 23.

It can be seen from Fig. 23 that the $CO_2$ absorption capacity decreased by 0.5966 mol $CO_2$ L$^{-1}$ after the first cycle, and then stabilized at about 1.6 mol $CO_2$ L$^{-1}$. In the simulated flue gas environment, the loading of $CO_2$ is about 75% of that in the pure $CO_2$ environment. After four absorption–desorption cycles, the total $CO_2$ cyclic loading of the MNBH was 5.21 mol $CO_2$ L$^{-1}$ absorbent, which had a better absorption effect and could be well applied to the decarbonization of flue gas in coal-fired power plants.

## 4.  Conclusion

In this paper, a new phase change absorbent MNBH was developed using MEA as the main absorbent, n-butanol as the phase separation promoter and water as the solvent, and the $CO_2$ absorption performance, desorption performance, phase separation behaviour, cyclic regeneration capacity and two-

phase material distribution of MNBH were explored and talked about, and the conclusions are as follows:

(1) Compared with the MEA phase change absorbent with *n*-propanol, isopropanol, and *tert*-butanol as phase separation promoters, the MNBH developed in this paper has higher $CO_2$ absorption capacity, smaller absorbent viscosity, and lower $CO_2$-rich phase volume.

(2) The optimum mass concentration of MEA was selected as 30 wt%. Fixing the mass concentration of MEA at 30 wt% and changing the mass ratio of *n*-butanol/$H_2O$, the MNBH absorbent had the strongest $CO_2$ absorption capacity of 2.5227 mol $CO_2$ $L^{-1}$ when the mass ratio of MNBH absorbent was 3 : 4 : 3. The $CO_2$ loading in the lower phase of the MNBH phase change absorbent was higher than 95% at all MNBH mass ratios.

(3) At the desorption temperature of 120 °C, the $CO_2$ desorption efficiency of the MNBH absorbent with a mass ratio of 3 : 4 : 3 reached 89.96%, and the energy consumption of $CO_2$ regeneration was 2.6 GJ $t^{-1}$ $CO_2$, which was about 35% lower than that of the 30 wt% MEA absorbent. The $CO_2$ absorption–desorption cycle experiments were carried out at an absorption temperature of 40 °C and a desorption temperature of 120 °C, and the results showed that the $CO_2$ cycling capacity increased and then decreased with the increase of *n*-butanol mass concentration. The highest $CO_2$ cycling capacity of 4.1918 mol $CO_2$ $L^{-1}$ was achieved at the MNBH mass ratio of 3 : 6 : 1, which was 72% higher than that of 30 wt% MEA absorbent. The $CO_2$ recycling capacity of the MNBH adsorbent with a mass ratio of 3 : 4 : 3 and the 30 wt% MEA absorbent was compared in four absorption–desorption cycles. The results showed that the total recycling capacity of the MNBH absorbent with a 3 : 4 : 3 mass ratio was 14.1672 mol $CO_2$ $L^{-1}$. It was 5.9752 mol $CO_2$ $L^{-1}$ higher than 30 wt% MEA absorbent. The MNBH absorbent has good recycling stability and is a promising $CO_2$ absorbent.

(4) FTIR and $^1H$ NMR results showed that the upper phase of MNBH was mainly composed of *n*-butanol, which was a $CO_2$-lean phase. The main components of the lower phase are MEA and carbamate, which is a $CO_2$-rich liquid phase. Experiments in simulated flue gas showed that the MNBH phase change absorbent has good potential for application in flue gas decarbonization in coal-fired power plants.

## Data availability

Data will be made available on request.

## Author contributions

Yanlong Hu: writing – original draft. Qiang Wang: funding acquisition. Dingkai Hu: data curation. Yingshuang Zhang: review & editing. Furqan Muhammad: data curation. Shijian Lu: aspenplus technical support.

## Conflicts of interest

The authors declare that they have no known competing financial interests or personal relationships that could have appeared to influence the work reported in this paper.

## References

1 S. Bachu, *Energy Convers. Manage.*, 2000, **41**, 953–970.
2 M. Li, G. Jia, Y. Zhao, X. Zhang and J. Zhao, *J. Chem. Eng.*, 2023, **74**, 365–379.
3 H. Yang, Z. Xu, M. Fan, R. Gupta, R. B. Slimane, A. E. Bland and I. Wright, *J. Environ. Sci.*, 2008, **20**, 14–27.
4 J. Rogelj, M. den Elzen, N. Höhne, T. Fransen, H. Fekete, H. Winkler, R. Schaeffer, F. Sha, K. Riahi and M. Meinshausen, *Nature*, 2016, **534**, 631–639.
5 N. Nakicenovic, *World Energy Outlook 2007: China and India Insights Paperback*, oecd publishing, 1st edn, 2007.
6 L. Duan, M. Zhao and Y. Yang, *Energy*, 2012, **45**, 107–116.
7 C. Zheng, J. Tan, Y. J. Wang and G. S. Luo, *Ind. Eng. Chem. Res.*, 2013, **52**, 12247–12252.
8 L. Hu, Phase transitional absorption method, *US Pat.*, 7541011, 2009.
9 Q. Zhuang, B. Clements, J. Dai and L. Carrigan, *Int. J. Greenhouse Gas Contro*, 2016, **52**, 449–460.
10 S. Liu, H. Ling, J. Lv, H. Gao, Y. Na and Z. Liang, *Ind. Eng. Chem. Res.*, 2019, **58**, 20461–20471.
11 J. Ye, C. Jiang, H. Chen, Y. Shen, S. Zhang, L. Wang and J. Chen, *Environ. Sci. Technol.*, 2019, **53**, 4470–4479.
12 M. W. Arshad, P. L. Fosbøl, N. von Solms, H. F. Svendsen and K. Thomsen, *J. Chem. Eng. Data*, 2013, **58**, 1974–1988.
13 A. F. Ciftja, A. Hartono and H. F. Svendsen, *Chem. Eng. Sci.*, 2013, **102**, 378–386.
14 Q. Huang, G. Jing, X. Zhou, B. Lv and Z. Zhou, *J. CO2 Util.*, 2018, **25**, 22–30.
15 G. Li, D. Deng, Y. Chen, H. Shan and N. Ai, *J. Chem. Thermodyn.*, 2014, **75**, 58–62.
16 K. Warmuzinski, M. Tanczyk and M. Jaschik, *Int. J. Greenhouse Gas Contro*, 2015, **37**, 182–190.
17 B. Wang, X. Chen and G. Yu, *Sep. Purif. Technol.*, 2022, **294**, 121173.
18 W. Zhang, X. Jin, W. Tu, Q. Ma, M. Mao and C. Cui, *Appl. Energy*, 2017, **195**, 316–323.
19 W. Zhang, X. Jin, W. Tu, *et al.*, *Energy Fuels*, 2017, **31**(4), 4273–4279.
20 Y. Shen, C. Jiang, S. Zhang, J. Chen, L. Wang and J. Chen, *Appl. Energy*, 2018, **230**, 726–733.
21 M. Xiao, W. Zheng, H. Liu, P. Tontiwachwuthikul and Z. Liang, *AIChE J.*, 2019, **65**, e16605.
22 R. Zhang, Q. Yang, B. Yu, H. Yu and Z. Liang, *Energy*, 2018, **144**, 1064–1072.
23 W. Tu, J. Fang, Z. Li, M. Mao, X. Jin, X. Liu and W. Zhang, *Sci. China: Chem.*, 2018, **48**, 641–647.

24 H. Hu, M. Fang, F. Liu, T. Wang, Z. Xia, W. Zhang, C. Ge and J. Yuan, *Appl. Energy*, 2022, **324**, 119570.

25 W. Jiang, F. Wu, G. Gao, X. Li, L. Zhang and C. Luo, *Chem. Eng. J.*, 2021, **420**, 129897.

26 M. Wang, M. Rahimi, A. Kumar, S. Hariharan, W. Choi and T. A. Hatton, *Appl. Energy*, 2019, **255**, 113879.

27 Z. Weifeng, Z. Wu and W. Qiuhua, *Prog. Chem. Chem. Ind.*, 2022, **41**(4), 2090–2101.

28 H. Kim, S. J. Hwang and K. S. Lee, *Environ. Sci. Technol.*, 2015, **49**, 1478–1485.

29 X. B. Zhou, *Doctoral Dissertation*, Huaqiao University, 2019.

30 B. Yu, H. Yu, K. Li, Q. Yang, R. Zhang, L. Li and Z. Chen, *Appl. Energy*, 2017, **208**, 1308–1317.

31 W. Zhao, Q. Zhao, Z. Zhang, J. Liu, R. Chen, Y. Chen and J. Chen, *Fuel*, 2017, **209**, 69–75.

32 X. Y. Luo, X. Fan, G. L. Shi, H. R. Li and C. M. Wang, *J. Phys. Chem. B*, 2016, **120**, 2807–2813.

33 G. Fan, A. Wee, R. Idem and P. Tontiwachwuthikul, *Ind. Eng. Chem. Res.*, 2009, **48**, 2717–2720.

34 F. Barzagli, F. Mani and M. Peruzzini, *Energy Environ. Sci.*, 2009, **2**, 322–330.

35 A. F. Ciftja, A. Hartono and H. F. Svendsen, *Int. J. Greenhouse Gas Control*, 2013, **16**, 224–232.

36 K. Zhu, H. Lu, C. Liu, K. Wu, W. Jiang, J. Cheng, S. Tang, H. Yue, Y. Liu and B. Liang, *Ind. Eng. Chem. Res.*, 2019, **58**, 3811–3821.